IEEE Access
Multidisciplinary | Rapid Review | Open Access Journal

Received May 11, 2022, accepted June 11, 2022, date of publication June 16, 2022, date of current version June 23, 2022.

Digital Object Identifier 10.1109/ACCESS.2022.3183801

Thermofluid-Solid Coupling Numerical Simulation Model of Blast Furnace Hearth Protection Measures

LEI WANG[1], LIANGYU CHEN[1], LEI ZHAO[1], YANG LI[2], AND JIAOCHENG MA[1]
[1]School of Mechanical Engineering and Automation, Northeastern University, Shenyang 110819, China
[2]State Key Laboratory of Intelligent Manufacturing of High-end Construction Machinery, Xuzhou 221004, China

Corresponding author: Lei Wang (1910079@stu.neu.edu.cn)

This work was supported in part by the Fundamental Research Funds for the Central Universities under Grant N180304020.

ABSTRACT The blast furnace hearth is the key position to determine the life of the blast furnace. To ensure the safety of the blast furnace hearth, when serious local depression erosion occurs in the hearth lining, necessary protection measures are taken to prevent the depression erosion from continuing to expand. At present, the measures and strength of furnace protection are mostly selected according to the engineering experience, lacking feasible theoretical methods to predict the effect of furnace protection. In this paper, a three-dimensional numerical model of thermofluid-solid coupling of blast furnace hearth with mushroom-type depression erosion was established. Taking hearth temperature and thermal stress as the evaluation indexes, the effect of furnace protection measures was predicted and evaluated. The influence of molten iron flow and the formation of a solidified iron layer on the temperature distribution of the refractory material was considered in the numerical model. We have verified the calculation model, and the calculated temperature value was in good agreement with the measured value. In addition, the numerical model was used to analyze common furnace protection measures such as increasing the furnace cooling, closing the tuyere, and reducing the smelting strength. The research results of this paper have guiding significance to select the type and strength of the blast furnace protection measures.

INDEX TERMS Blast furnace hearth, furnace protection measures, numerical simulation, solidification and melting, thermal stress.

NOMENCLATURE

C	Inertial resistance coefficient.
ϖ	Porosity.
d_c	Average diameter of the coke in the deadman.
T	Temperature.
$\lambda(T)$	Thermal conductivity of materials at different temperatures.
H	Total enthalpy of the substance.
h	Sensible heath enthalpies.
ΔH	Latent heath enthalpies.
ρ	Fluid density.
u	Fluid velocity.
S	Source term.
L	Latent heat of the material.
T_{solid}	Fluid solidification temperature.
T_{liquid}	Fluid melting temperature.
T_0	Initial temperature.
$\sigma_i(\mathrm{i} = x, y, z)$	Components of the thermal stress parallel to the x, y, and z-axes.
$\varepsilon_i(\mathrm{i} = x, y, z)$	Components of the thermal strain parallel to the x, y, and z-axes.
$\tau_{xy}, \tau_{yz}, \tau_{zx}$	Components of the shear stress.
u, v, w	Displacement components.
E	Tensile and compressive modulus of elasticity.
μ	Poisson's ratio.
α	Coefficient of thermal expansion.

The associate editor coordinating the review of this manuscript and approving it for publication was Gang Mei.

I. INTRODUCTION

The blast furnace (BF) is an important type of ironmaking equipment, and its production life determines its economic benefits. Production practice has shown that the life of a BF

TABLE 1. Examples of hearth burnthrough accidents [13].

Blast furnace code	Hearth diameter(m)	Burnthrough time
Azovztal, Ukraine No.3	9.4	Aug. 2006
TKS, Schwelgen No.1	13.6	Nov. 2006
Cones Port Talbot No.4	11.5	Nov. 2006
Areclor Mittal-Sicatsa No.1	9.0	Jun. 2007
US Steel Gary No.14	12	Apr. 2009
Salzgitter No.B	11.2	Mar. 2010
Dillingen No.5	12.0	Jun. 2010

depends on its hearth in a bad working environment [1]–[4]. During the BF production process, the refractory lining of the hearth comes into direct contact with high-temperature molten iron. As a result of molten iron erosion, alkali metal corrosion, and thermal stress, irreversible local depression erosion occurs in the hearth [5]–[8]. If the erosion continues to develop, burnthrough accidents will occur, resulting in severe casualties and causing extensive property loss for the business. It is critical to ensure that the BF hearth is safe. Some examples of hearth burn-through accidents are listed in Table 1.

For many years, scholars have been working to model the ironmaking process in BFs. The research methods include laboratory tests and numerical simulations [9]–[12]. At present, it is common to disassemble and study BFs after the end of service [14], [15]. With the development of computer hardware and numerical calculations, computer simulations have become a feasible alternative method. Zhao *et al.*. studied the phenomenon of molten iron solidification in hearths to form a solidified iron layer for the first time with comprehensive numerical simulations of heat transfer, fluid dynamics, and solidification [16]. A two-dimensional computational fluid dynamics model was established based on heat transfer fluid dynamics and the solidification and melting model. The influence of parameters such as the lining performance and structure, cooling water temperature and flow rate, molten iron yield, and temperature on the formation of a solidified iron layer was studied. The research results show that a combined structure consisting of carbon bricks and graphite bricks can promote the formation of a solidified iron protective layer, and measures such as reducing productivity, closing the tuyere, and lowering the temperature of the molten iron can effectively slow the development of hearth depression erosion.

Komiyama *et al.*. established a computational fluid dynamics model that improved turbulence modeling, wall boundary processing, and mesh resolution [17]. The calculation model predicted the flow and temperature distribution of the molten iron in the BF hearth as well as the temperature distribution of the refractory materials. Four typical situations in the hearth were simulated and calculated, and the distribution of the molten iron flow in the intact hearth, corroded hearth, sitting coke bed, and floating coke bed were discussed.

To investigate the thermal stress of a hearth with depression erosion, Chen *et al.*. established a two-dimensional thermal-solid coupling model to study the thermal stress distribution of the hearth under three typical depression erosion conditions [18]. The results show that thermal stress is the main cause of erosion development. The thermal stress of a bowl-type erosion hearth is small and uniform, and the hearth is in a stable state. For mushroom-type and elephant-foot-type erosion hearths, increasing the cooling strength can reduce the thermal shock caused by the molten iron, promote the formation of a protective layer of solidified iron, and extend the production life of the hearth.

To ensure the safety of the hearth, some measures can be taken to protect the hearth to slow the expansion of the local depression erosion and prevent serious safety accidents caused by hearth burn-through [19], [21]. At present, most furnace protection measures are selected according to engineering experience, and no feasible method exists to evaluate and predict the effects of furnace protection.

In previous work, we established a three-dimensional thermofluid coupling numerical model of BF hearth with an ''elephant-foot-type'' depression erosion [22]. The phase transition behavior of molten iron solidification was considered in the computational model. Using the calculation model, the thickness of the solidified iron layer is used as the evaluation index to evaluate the effectiveness of the common furnace protection measures. In this paper, the thermal stress of BF hearth with depression erosion was studied. Based on the original research results, a thermal stress analysis module was added to the simulation model in this paper, and the research object was replaced by a BF hearth with a complex structure. A 3D numerical model of thermofluid-solid coupling of BF hearth with ''mushroom-type'' depression erosion was established, and the temperature distribution and thermal stress distribution of the hearth in various production states were analyzed. The calculation model accounts for molten iron flow and the formation of a solidified iron protective layer, and the calculation results are similar to the actual production state. The calculation model was verified by comparing the simulated and measured values of the thermocouple temperature. In addition, the calculation model was applied to evaluate the effectiveness of common furnace protection measures, such as reducing the smelting strength, increasing the cooling strength, and closing the tuyere [23], [28].

II. MODELS AND METHODS

In this paper, a 3D model of a BF hearth with mushroom-type depression erosion was established by using SolidWorks software, and a numerical simulation model of thermofluid-solid coupling of the hearth was established based on the commercial software Ansys Workbench multi-physical field coupling platform. The calculation model was divided into two parts. First, a mathematical model combining numerical simulations of heat transfer, fluid dynamics, and solidification was established by using the Fluent module. The flow of the molten iron in the hearth and the coupled heat transfer between the molten iron and refractory material were simulated and calculated, and the temperature distribution of the refractory material in the hearth was obtained. The refractory temperature calculated

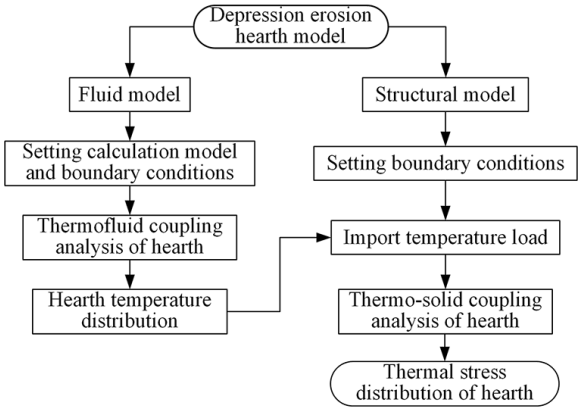

FIGURE 1. The calculation process of the thermofluid-solid coupling model for the BF hearth.

by Fluent was loaded into the static analysis module, and the thermal stress of the hearth was analyzed. Since the molten iron pressure has little effect on the structural stress, the calculation model only considers the effect of the temperature on the stress of the hearth. The calculation process of the thermal stress analysis of the hearth is shown in Fig. 1. A detailed description of the calculation models for each part is given below.

A. PHYSICAL MODELS

The effective volume of the BF was 3200 m^3, and the refractory material of the hearth was a ceramic cup-carbon brick structure. As shown in Fig. 3(a), the lining of the hearth contained six kinds of carbon bricks: high thermal conductivity graphite brick, ultramicroporous carbon brick, SGL carbon brick, molded small carbon brick, and microporous carbon brick. The inner diameter of the taphole of the hearth was 250 mm, and the included angle with the horizontal direction was 10°. During BF production, a certain amount of stemming was injected into the hearth through the taphole after each tapping. The stemming formed a convex mud bag that was attached to the inner side of the hearth near the taphole to protect the furnace wall. In this paper, stemming was simplified by using a circular platform with a height of 1000 mm. The physical properties of the refractories and molten iron in the calculation model are listed in Table 2, where T is the temperature, indicating that the property value changes with the temperature. In addition, "–" represents that the material does not have this property.

The local depression erosion of the hearth lining often occurs in the furnace corner area, with a majority in the direction of a 30°–60° angle with the taphole. Therefore, a "mushroom-type" lining depression was constructed in this study. It is in the hearth corner area with an azimuth angle of 45° from the taphole. The hearth lining erosion profile is shown in Fig. 3(b), and the 3D physical model of the hearth is shown in Fig. 2.

In the continuous production process of the blast furnace, a substantially immobile column of coke is formed in the center of the hearth, which is called a deadman [29], [30]. The whole

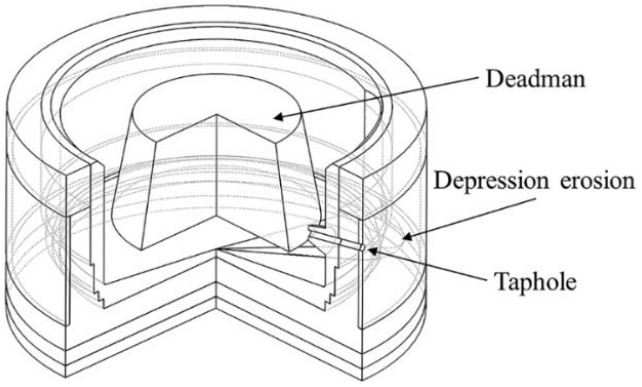

FIGURE 2. 3D model of the mushroom-type erosion hearth.

of the deadman is conical, the lower part is immersed in the liquid slag iron, and the upper spire is located in the blast furnace bosh. The blast furnace bosh area was not considered in the calculation model of this paper, so the deadman was represented by a frustum of a cone. The porous medium model was used to reflect the effect of the deadman on the flow of the molten iron [31]–[35]. According to the Ergun equation and Darcy's law, the source term of the kinetic loss caused by a single and homogeneous porous medium consists of viscous loss term and inertial loss term, as shown in (1) and (2).

$$\frac{1}{\alpha} = \frac{150}{d_c^2}\frac{(1-\varpi)^2}{\varpi^3} \tag{1}$$

$$C = \frac{3.5}{d_c}\frac{(1-\varpi)}{\varpi^3} \tag{2}$$

where $1/\alpha$ is the viscous resistance coefficient; C is the inertial resistance coefficient; ϖ is the porosity, which was taken as 0.3 in the calculation model; and d_c is the average diameter of the coke in the deadman, which was taken as 0.03 m in the calculation model [34].

B. GOVERNING EQUATION

BF ironmaking is a continuous process. The hot iron generated in the BF is continuously gathered to the hearth and discharged from the taphole [36]. The calculation model assumes that the molten iron is an incompressible viscous fluid and uses the k-epsilon turbulence model to simulate the flow of the molten iron [37], [38]. Because the heat generated by the heat radiation of the hearth is relatively small, the influence of the heat radiation can be ignored in the calculation model.

1) HEAT CONDUCTION DIFFERENTIAL EQUATION

In this study, the coupled heat transfer process of the molten iron and refractory in the hearth can be described by the differential equation of heat conduction, as shown in (3).

$$\frac{\partial}{\partial x}\left[\lambda(T)\frac{\partial T}{\partial x}\right] + \frac{\partial}{\partial y}\left[\lambda(T)\frac{\partial T}{\partial y}\right] + \frac{\partial}{\partial z}\left[\lambda(T)\frac{\partial T}{\partial z}\right] = 0 \tag{3}$$

where T is the temperature and $\lambda(T)$ is the thermal conductivity of materials at different temperatures.

TABLE 2. Physical properties of solid materials and molten iron.

Materials	Microporous carbon brick	Molded small carbon brick	Microporous corundum brick	Ultramicroporous carbon brick	SGL carbon brick	Graphite brick	Molten iron
Density (kg/m^3)	1620	1750	3320	1750	1730	1780	6700
Specific heat (J/(kg·K))	840	840	840	840	840	840	756
Thermal conductivity (W/(m·K))	$8.88 + 0.0044T$	18	4.53	22.81	22.5	$46.61 - 0.01342T$	$0.0158T$
Young's modulus (GPa)	7.9	7.9	25	7.9	9.3	7.9	–
Poisson's ratio	0.15	0.15	0.25	0.15	0.15	0.15	–
Coefficient of thermal expansion (10^{-6}/°C)	2.84	2.8	2.14	3.32	2.7	2.16	–
Viscosity (kg/(m·s))	–	–	–	–	–	–	0.007
Melting heat (J/kg)	–	–	–	–	–	–	103343
Solidification temperature (K)	–	–	–	–	–	–	1423
Melting temperature (K)	–	–	–	–	–	–	1573

2) SOLIDIFICATION AND MELTING MODEL

Under forced cooling of the external cooling system of the hearth, the temperature of the molten iron near the lining decreases. When the molten iron temperature is lower than 1150 °C, the molten iron condenses and adheres to the hot surface of the inner liner, forming a solidified iron protective layer [39], [40]. In this paper, the solidification and melting model was used to simulate the formation of the solidified iron layer in the hearth [41], [42]. The enthalpy-porosity technique was used to simulate the fluid solidification and melting process. The pressure drop due to the presence of solid materials was simulated by adding a source term to the momentum equation. The energy equation of the solidification and melting model is as follows:

$$\frac{\partial(\rho H)}{\partial t} + \nabla \cdot (\rho u H) = \nabla \cdot (\lambda \nabla T) + S \tag{4}$$

where H is the total enthalpy of the substance, $H = h + \Delta H$, which includes the sensible (h) and latent (ΔH) heath enthalpies; ρ is the fluid density; u is the fluid velocity; and S is the source term. The latent heat (ΔH) is an important parameter for determining the effect of solidification that can be described as a function of the liquid fraction.

$$\Delta H = \varpi L \tag{5}$$

where L is the latent heat of the material. When the fluid is completely solid, the porosity decreases to 0, and the flow rate of the corresponding region also decreases to 0. When the fluid is completely melted, the porosity increases to 1, but the fluid flow in the corresponding region is not affected. The porosity of the liquid-solid paste zone is between 0 and 1. The porosity at different temperatures can be calculated as:

$$\begin{cases} \varpi = 0 & \text{if} \quad T < T_{solid} \\ \varpi = 1 & \text{if} \quad T > T_{liquid} \\ \varpi = \frac{T - T_{solid}}{T_{liquid} - T_{solid}} & \text{if} \quad T_{solid} < T < T_{liquid} \end{cases} \tag{6}$$

where T_{solid} is the fluid solidification temperature and T_{liquid} is the fluid melting temperature.

3) STRESS MODEL

According to thermoelastic theory, the thermal deformation behavior of the hearth can be described by the following equations [43]. Equations (7)–(9) are the equilibrium equation, kinematic equation, and constitutive equation, respectively.

$$\begin{cases} \frac{\partial \sigma_X}{\partial x} + \frac{\partial \tau_{yx}}{\partial y} + \frac{\partial \tau_{zx}}{\partial z} = 0 \\ \frac{\partial \tau_{xy}}{\partial x} + \frac{\partial \sigma_y}{\partial y} + \frac{\partial \tau_{zy}}{\partial z} = 0 \\ \frac{\partial \tau_{xz}}{\partial x} + \frac{\partial \tau_{yz}}{\partial y} + \frac{\partial \sigma_z}{\partial z} = 0 \end{cases} \tag{7}$$

$$\begin{cases} \varepsilon_x = \frac{\partial u}{\partial x}, \gamma_{xy} = \frac{\partial u}{\partial y} + \frac{\partial v}{\partial x} \\ \varepsilon_y = \frac{\partial v}{\partial y}, \gamma_{yz} = \frac{\partial v}{\partial z} + \frac{\partial w}{\partial y} \\ \varepsilon_z = \frac{\partial w}{\partial z}, \gamma_{zx} = \frac{\partial u}{\partial z} + \frac{\partial w}{\partial x} \end{cases} \tag{8}$$

$$\begin{cases} \varepsilon_x = \frac{1}{E}\left[\sigma_x - \mu\left(\sigma_y + \sigma_z\right)\right] + \alpha\left(T - T_0\right), \gamma_{yz} = \frac{2(1+\mu)}{E}\tau_{yz} \\ \varepsilon_y = \frac{1}{E}\left[\sigma_y - \mu\left(\sigma_x + \sigma_z\right)\right] + \alpha\left(T - T_0\right), \gamma_{zx} = \frac{2(1+\mu)}{E}\tau_{zx} \\ \varepsilon_z = \frac{1}{E}\left[\sigma_z - \mu\left(\sigma_x + \sigma_y\right)\right] + \alpha\left(T - T_0\right), \gamma_{xy} = \frac{2(1+\mu)}{E}\tau_{xy} \end{cases} \tag{9}$$

where T_0 is the initial temperature; σ_i(i $= x, y, z$) are the components of the thermal stress parallel to the x, y, and z-axes; ε_i(i $= x, y, z$) are the components of the thermal strain parallel to the x, y, and z-axes; τ_{xy}, τ_{yz}, τ_{zx} and γ_{xy}, γ_{yz}, γ_{zx} are the components of the shear stress; u, v and w are the displacement components; E is the tensile and compressive modulus of elasticity; μ is Poisson's ratio, and α is the coefficient of thermal expansion.

C. BOUNDARY CONDITIONS

In the thermofluid coupling model, the top inlet of the hearth was an annular region due to the presence of a deadman in the center of the hearth, as shown in Fig. 3(b). The inlet temperature of the molten iron in the calculation model was held constant at 1803 K. According to the effective volume of the BF and the volume utilization coefficient, the mass flow rate of the inlet is 90 kg/s. The taphole is used as the outlet of the calculation model.

The thermal boundary conditions of the computational model were as follows. Cooling equipment was required to

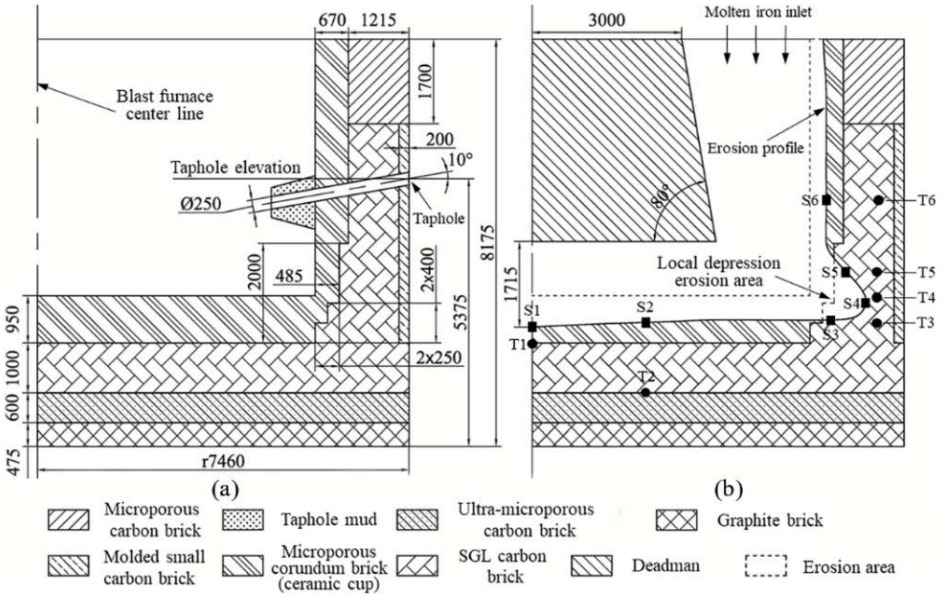

FIGURE 3. Schematic diagram of the BF hearth structure and depression erosion. (a) the design structure of hearth lining; (b) hearth erosion profile.

protect the shaft and shell during BF production, and cooling staves made of cast iron or copper were usually arranged between the hearth and shell. In this paper, the cooling structure was not established in the 3D structure model. In the thermofluid coupling calculation model, the convection heat transfer coefficient (h_c) of the side walls of the hearth were equivalent and calculated by using the convection heat transfer boundary replacement method of the long cylinder [44], [45]. The equivalent convection heat transfer coefficient of the sides wall of the hearth was calculated by (10)–(13). The convection heat transfer coefficient of the furnace bottom was 60 W/(m^2·K) [46], and all other boundaries were adiabatic boundaries.

$$h_w = 208.8 + 47.5v_w \tag{10}$$

$$h_1 = \gamma h_w \tag{11}$$

$$h_2 = \frac{r_1}{r_2}\frac{h_1\lambda_1}{\lambda_1 + h_1 r_1 \ln\left(r_1/r_2\right)} \tag{12}$$

$$h_c = \frac{r_2}{r_3}\frac{h_2\lambda_2}{\lambda_2 + h_2 r_2 \ln\left(r_2/r_3\right)} \tag{13}$$

where h_w is the convection heat transfer coefficient of the surface of the cooling wall water pipe; v_w is the flow rate of the cooling water; h_1 is the equivalent convection heat transfer coefficient of the central surface of the cooling wall water pipe; γ is the cooling specific surface area; h_2 is the equivalent convection heat transfer coefficient of the cold surface of the packing layer; r_1 is the distance from the center of the cooling water pipe to the center of the hearth; r_2 and r_3 are the inner diameter and outer diameter of the packing layer, respectively; λ_1 is the heat conduction coefficient of the cooling wall, and λ_2 is the thermal conductivity of the packing.

In the stress analysis model of the hearth, the fluid domain component of the calculation model was suppressed, and only the refractory part of the hearth was retained. The cooling wall and shell on the outside of the hearth have the effect of circumferentially supporting the hearth, so x-axis and y-axis displacement constraints are added to the outside of the hearth. A z-axis direction displacement restriction was added to the bottom of the hearth. For the top of the hearth, z-axis direction displacement and deformation consistent constraint conditions are set. The reference temperature was set to 25 °C.

III. RESULTS AND DISCUSSION

The simulation model of the hearth was used to analyze furnace measures such as reducing the smelting strength, increasing the cooling strength, and closing the tuyere. In the BF studied in this paper, 35 thermocouple measurement points were arranged on the erosion cross-section, with six points selected as temperature monitoring points. Six stress monitoring points were arranged on the erosion boundary of the refractory material. The positions of the monitoring points are shown in Fig. 3(a), where T1–T6 are the temperature monitoring points and S1–S6 are the stress monitoring points. The maximum principal stress theory was used to evaluate the thermal stress of the refractories. The effects of several common furnace protection measures on the local depression erosion of the hearth were evaluated by the temperature and thermal stress changes in the hearth.

A. MODEL VERIFICATION

First, the mesh independence of the computational model was verified. In this paper, the computational model was discretized using tetrahedral grids. Meshes with relatively small geometric sizes at the local depression erosion area and

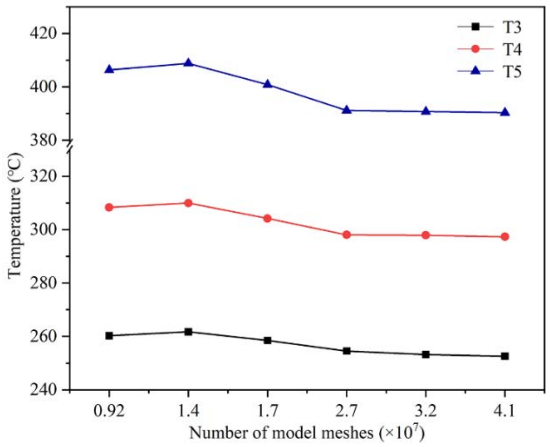

FIGURE 4. The temperature of monitoring points with different mesh.

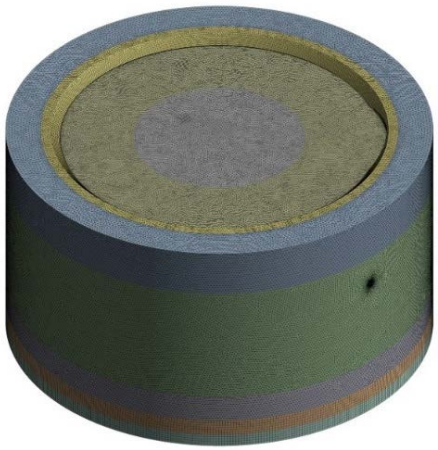

FIGURE 5. The mesh of the computational model.

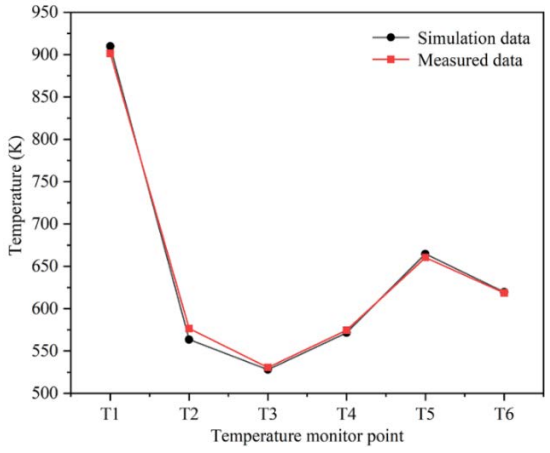

FIGURE 6. Comparison between simulated and measured temperature values at the temperature monitoring points.

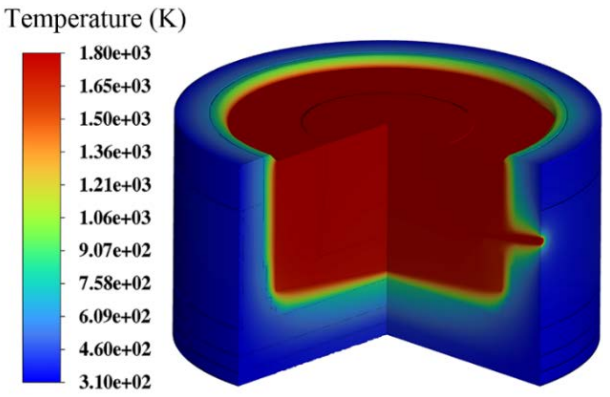

FIGURE 7. Temperature distribution of hearth.

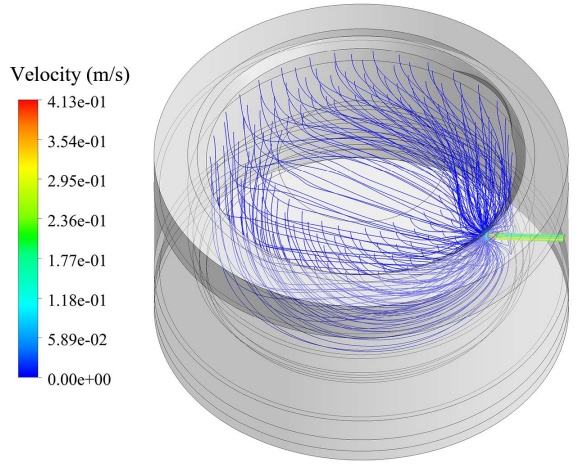

FIGURE 8. Streamline of molten iron.

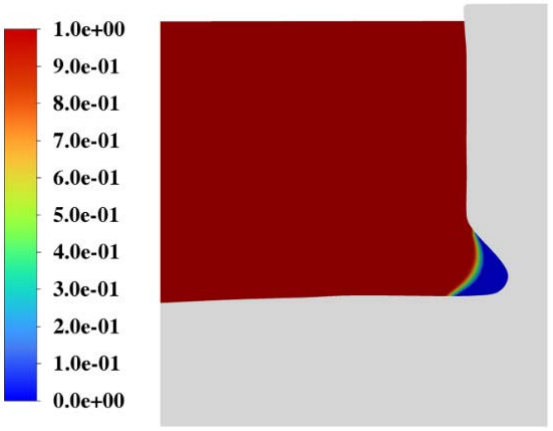

FIGURE 9. The volume fraction of molten iron in the erosion cross-section.

the taphole were densified, with their size being one-third of the mesh size of the rest of the fluid domain. To improve the convergence of the calculation model, five layers of expansion mesh were arranged at the interface between the molten iron and the hearth. As shown in Fig. 4, when the number of meshes reaches 2.7×10^7, the temperature change at each monitoring point is less than 2%, indicating that the calculation result is no longer affected by the number of meshes. Therefore, the calculation model adopts the fourth grid division method, which not only maintains the calculation accuracy but also improves the calculation efficiency. The divided mesh model is shown in Fig. 5.

Then, the accuracy of the simulation results was verified. The cooling specific surface area of the BF hearth cooling stave was 1.48. The distance from the center of the cooling water pipe to the hot surface of the cooling wall was

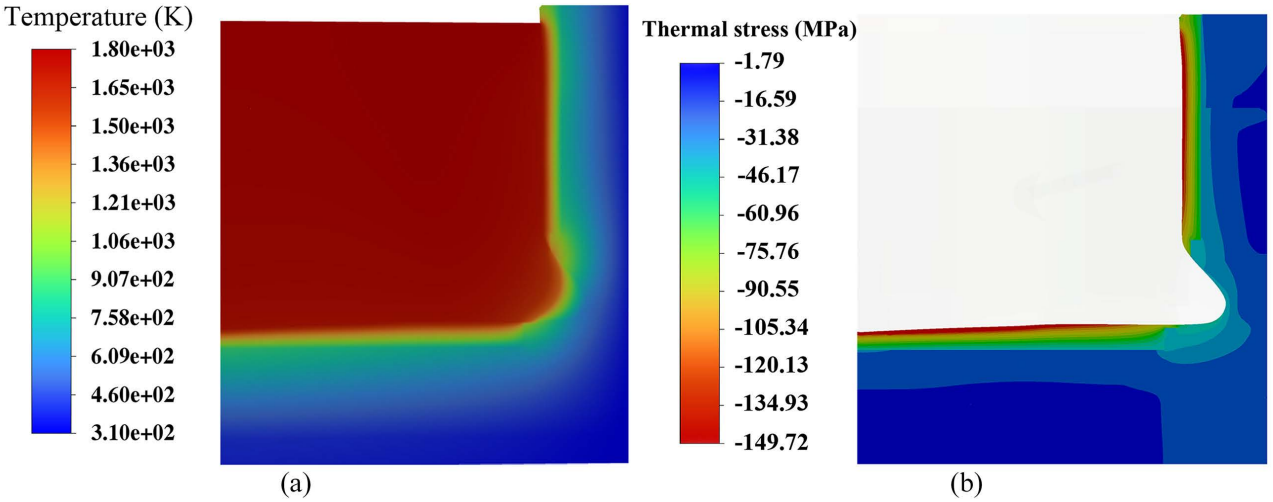

FIGURE 10. Temperature and thermal stress distributions on the erosion cross-section. (a) temperature distribution; (b) thermal stress distribution.

80 mm. The thickness of the packing layer was 100 mm. The cooling water flow rate in the cooling wall was 1.5 m/s. The equivalent convection heat transfer coefficient of the side wall was calculated as 120.0 W/(m^2·K). Fig. 6 shows a comparison between the calculation model and the actual production of the temperature at each monitoring point. The figure shows that the errors between the simulated and measured temperature values at each temperature measuring point are small, and the errors are controlled to within 2.25%. This shows that the calculation model is close to the actual production state of the hearth, which proves the reliability of the calculation results.

B. NORMAL PRODUCTION STATE CALCULATION RESULT

The normal production state (without furnace protection measures) was calculated. The calculated temperature distribution of the hearth is shown in Fig. 7. The overall temperature of the hearth gradually decreases from the inside to the outside under the action of the outside cooling system of the hearth. This temperature distribution provides the conditions for forming a solidified iron protective layer inside the hearth.

The streamline of the molten iron inside the hearth is shown in Fig. 8. Because the deadman in the hearth impedes the flow of molten iron, most of the molten iron flows from the surrounding and bottom of the deadman, and the molten iron forms a circulation phenomenon inside the hearth. In addition, almost no molten iron flows through the depression erosion area, which indicates that a solidified iron layer has formed under the current production conditions. Fig. 9 shows the volume fraction of the molten iron in the cross-section where the depression is eroded. The volume fraction of the molten iron near the erosion area is 0, indicating that a solidified iron layer has formed at this location. As the lining of the hearth erodes, the side wall of the hearth in the corresponding position becomes thinner, and the thermal resistance of the eroded area decreases. Under the same cooling conditions, the cooling rate of molten iron at this position is faster, which is more conducive to the formation of the solidified iron layer. Therefore, under normal production conditions, the erosion area of the hearth can form a protective layer of solidified iron to prevent the further expansion of the erosion.

The temperature distribution of the depression erosion cross-section is shown in Fig. 10(a). The refractory temperature gradually decreases from the inside to the outside, and the high-temperature area is mainly concentrated on the ceramic cup. The refractory temperature differs significantly between the ceramic cup and the carbon brick. The reason for this is that the thermal conductivity of the ceramic cup is low, which prevents the heat generated by the molten iron from transferring to the carbon brick. Although there is no ''protection'' of the ceramic cup in the erosion area, the temperature of the carbon brick near the erosion area is significantly reduced due to the presence of the solidified iron layer with a lower thermal conductivity. Fig. 10(b) shows the thermal stress distribution of the erosion cross-section. The overall stress distribution is high inside and lows outside. The high-temperature area of the ceramic cup has large thermal stress. The ceramic cups effectively protect the carbon bricks. The overall thermal stress of the carbon bricks in the recessed erosion area is relatively small and gradually decreases in a diffused state.

C. THE EFFECT OF THE TAPPING PRODUCTIVITY ON DEPRESSION EROSION

Reducing tapping productivity is an effective method for alleviating the erosion of the hearth lining [47]. To study the effect of tapping productivity on local depression erosion, a comparative simulation model was established based on the calculation model of BF normal production. The inlet mass flow rates of each simulation model were 70 kg/s, 80 kg/s, 90 kg/s (normal production state), 100 kg/s, 110 kg/s, and 120 kg/s. The other parameters were consistent with the normal production state model.

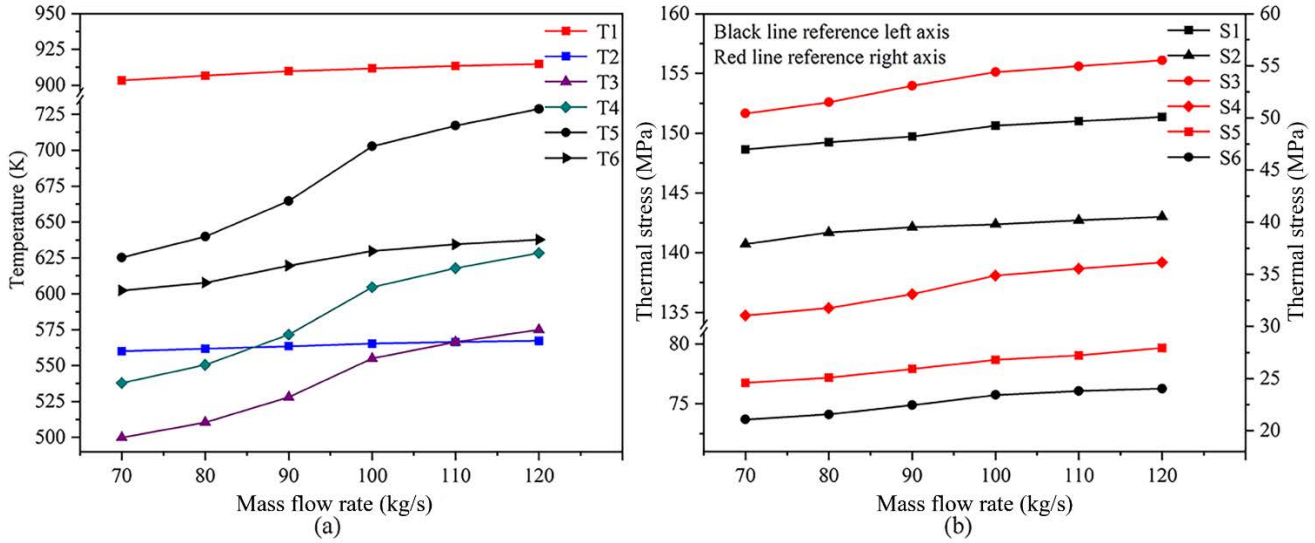

FIGURE 11. The effect of the tapping productivity on the temperature and thermal stress distributions of the hearth. (a) temperature; (b) thermal stress.

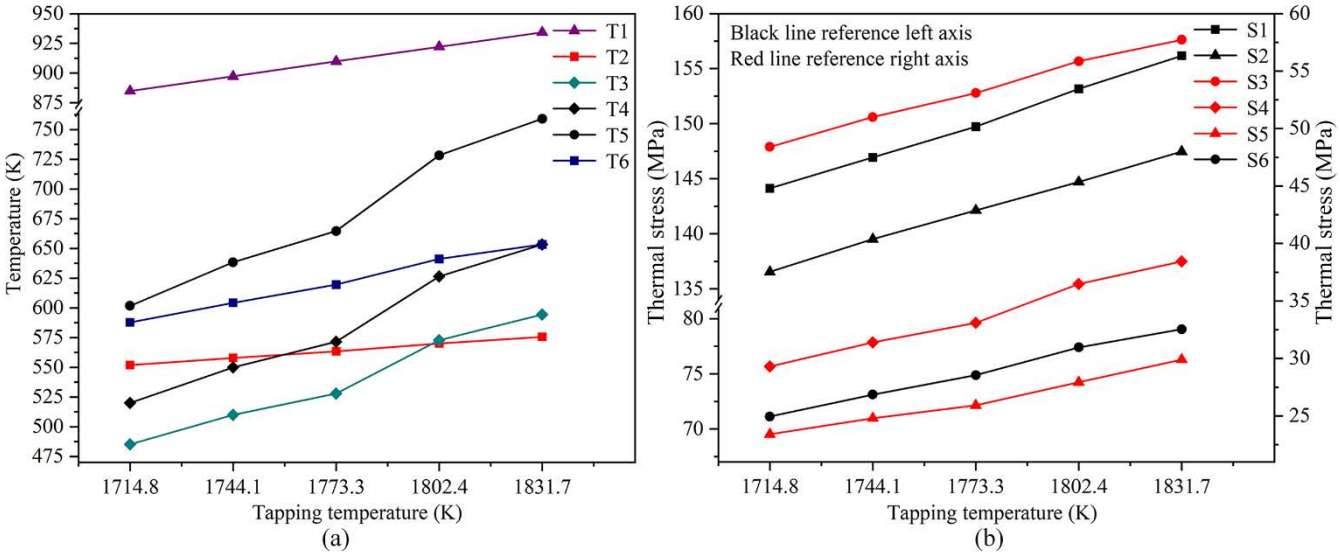

FIGURE 12. The effect of the tapping temperature on the temperature and thermal stress distributions of the hearth. (a) temperature; (b) thermal stress.

The effect of tapping productivity on the hearth temperature is shown in Fig. 11(a). Overall, as productivity increases, the temperature at each temperature measurement point increases. The temperature change at the bottom of the hearth was relatively small, and the temperature at T1 and T2 increased by 11.5 K and 7.2 K, respectively. The temperature change in the depression erosion area was the largest, with the temperatures at T3, T4, and T5 increasing by 75.1 K, 90.5 K, and 103.5 K, respectively. In addition, with increasing productivity, the temperature change rate in the erosion area decreases. Increased productivity causes an increase in the flow rate of the molten iron, which transfers more heat to the refractory material, increasing the temperature of the refractory material. At the same time, the increased molten iron velocity is not conducive to the formation of the solidified iron layer, resulting in a thin solidified iron layer, which reduces the protective effect of the solidified iron layer on depression erosion. Under the simultaneous action of the two factors, the temperature increase in the erosion area of the hearth is particularly large.

Fig. 11(b) shows the effect of tapping productivity on the thermal stress of the hearth. The stress in the furnace bottom is relatively high, while the stress in the depression erosion area is relatively low. With increasing productivity, the stress at each monitoring point increases, with the stress in the erosion area changing the most and the stresses at S3 and S4 increasing by 5.1 MPa. With increasing productivity, the change rate of stress decreases. It can be seen from the above analysis that as the productivity of the BF decreases, the temperature and stress of the depression

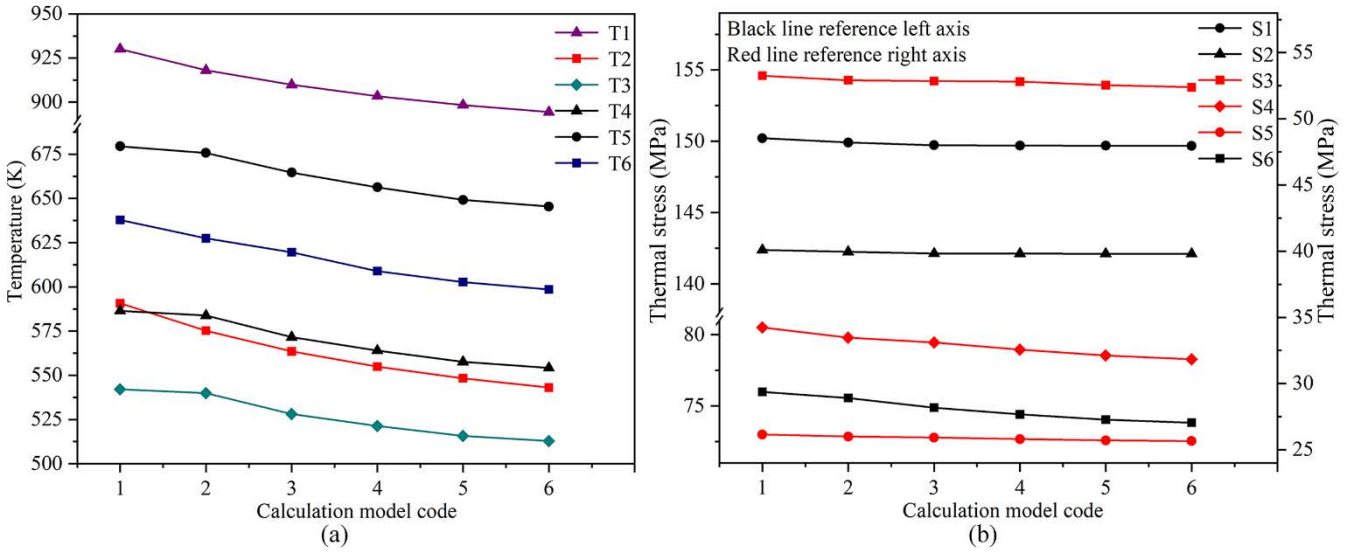

FIGURE 13. The effect of the cooling strength on the temperature and thermal stress distributions of the hearth. (a) temperature; (b) thermal stress.

erosion decrease to a certain extent, which effectively prevents the development of local depression erosion. Under the premise of meeting the production demand, productivity can be appropriately reduced to prolong the operation life of the BF.

D. THE EFFECT OF THE TAPPING TEMPERATURE ON DEPRESSION EROSION

The internal temperature of the hearth has a great influence on the local depression erosion of the lining. Because the internal temperature of the hearth is high, it is impossible to measure directly. In this study, five different tapping temperature calculation models were simulated. The tapping temperatures were 1714.8 K, 1744.1 K, 1773.3 K, 1802.4 K, and 1831.7 K, where 1773.3 K is the tapping temperature in the normal production model. The other parameters were consistent with the normal production state model.

The effect of the tapping temperature on the hearth temperature is shown in Fig. 12(a). With increasing tapping temperature, the temperature at each temperature monitor point increases. The temperatures at T1 and T2 in the bottom of the hearth increased by 49.4 K and 23.7 K, respectively. The temperature change in the depression erosion area was the largest, with the temperatures at T3, T4, and T5 increasing by 109.3 K, 133.4 K, and 157.3 K, respectively. The molten iron is a direct source of heat in the hearth. As the tapping temperature rises, the total heat in the hearth increases, resulting in an overall increase in the hearth temperature. At the same time, because the whole furnace temperature rises, the thickness of the solidified iron layer becomes thinner, resulting in a large change in the temperature of the erosion area. The temperature variation at each position of the hearth is arranged from small to large as follows: bottom area, sidewall area, and depression erosion area. In addition, as the tapping temperature increases, the temperatures in the bottom and the side walls of the hearth increase linearly,

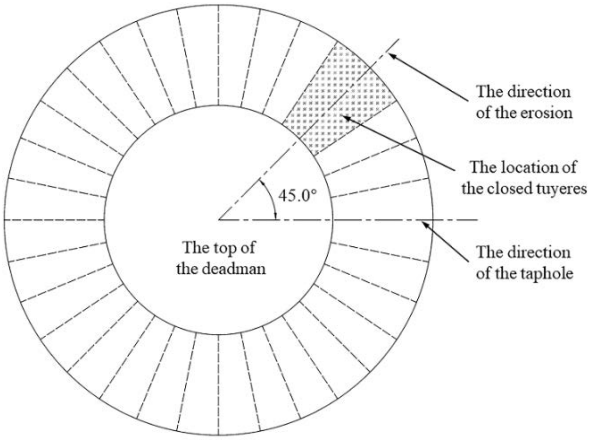

FIGURE 14. The positions of BF tuyeres.

while the temperature change rate in the erosion area becomes increasingly larger.

Fig. 12(b) shows the effect of the tapping temperature on the thermal stress of the hearth. The stress in the bottom of the hearth is relatively high, while the stress in the depression erosion area is relatively low. In addition, as the tapping temperature increases, the stress value at each monitoring point increases approximately linearly. The stress variations in the bottom area of the hearth and the depression erosion area are both approximately 10 MPa. From the above analysis, it can be seen that the tapping temperature has a great influence on the overall temperature and stress state of the hearth. Because the tapping temperature is related to the active degree of the BF hearth and the subsequent transportation of molten iron, under the premise of ensuring the active production of the BF, reasonably reducing the tapping temperature has a significant effect on slowing the erosion development rate and effectively extending the safe working life of the hearth.

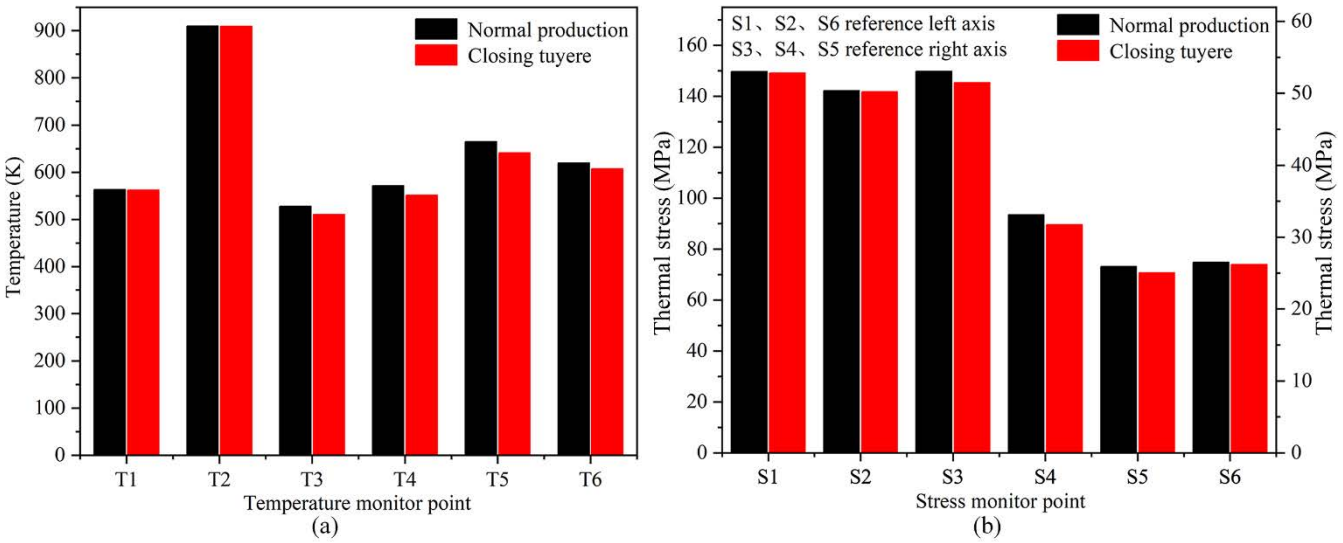

FIGURE 15. The effect of closing the tuyeres on the temperature and thermal stress distributions of the hearth. (a) temperature; (b) thermal stress.

TABLE 3. The convection heat transfer coefficients of each calculation model. (W/(m^2·K)).

Model code	1	2	3	4	5	6
Sidewall	80	100	120	140	160	180
Bottom	40	50	60	70	80	90

E. THE EFFECT OF THE COOLING INTENSITY ON DEPRESSION EROSION

Cooling equipment was arranged on the outside and bottom of the hearth to transfer the heat in the BF to the environment through cooling water to cool the hearth lining and alleviate the erosion of molten iron in the lining. During the actual production process, the cooling strength of the hearth is affected by many factors, including the cooling water flow, the structure of the brickwork, the scaling of the cooling wall, and the formation of an air gap in the hearth. In this section, the influence of different cooling intensities on the local depression erosion was analyzed, and six groups of test models were established. The other parameters were kept the same as in the normal production state model, with only the convection heat transfer coefficients of the side walls and bottom of the hearth changing. The convection heat transfer coefficient values for each calculation model are shown in Table 3. The third group is the normal production model.

The influence of the cooling intensity on the hearth temperature is shown in Fig. 13(a). The temperature at each temperature monitoring point gradually decreases with increasing cooling intensity. The temperature changes in all areas of the hearth are essentially the same, ranging from 30 K to 50 K. As the cooling intensity increases, the heat exchange between the hearth and the external environment increases, resulting in a decrease in the overall temperature of the hearth. It is worth noting that as the cooling intensity increases, the temperature change at each temperature monitoring point gradually slows, which indicates that the influence of the cooling intensity on the temperature of the hearth decreases as the cooling intensity increases.

Fig. 13(b) shows the relationship between the cooling intensity and the thermal stress of the hearth. It can be seen that with increasing cooling strength, the stress at each monitoring point decreased to a certain extent. Due to the small temperature variation of the hearth caused by the change in the cooling strength, the stress variation range of each region of the hearth is also small. The maximum stress change occurs in the middle of the erosion area, with the stress decreasing by 2.5 MPa at S4. In additon, the change in the stress in the erosion area decreases with increasing cooling strength. In summary, increasing the cooling intensity has a certain relieving effect on the depression erosion of the hearth. When the cooling strength increases to a certain point, the temperature and stress of the hearth are no longer sensitive. In order to save resources, it is necessary to match the appropriate cooling intensity for the hearth.

F. THE EFFECT OF CLOSING THE TUYERES ON DEPRESSION EROSION

The closing part of the tuyeres is one of the commonly used furnace protection methods. The tuyere is mainly used to blow hot air and pulverized coal into the BF to provide auxiliary fuel for the chemical reaction. Closing the tuyere weakens the chemical reaction in the corresponding area and reduces the amount of locally generated iron. The tuyere position of the BF studied in this paper is shown in Fig. 14. In the calculation model, the inlet was evenly divided according to the position of the tuyere, and the mass flow rate of each inlet was separately loaded. The mass flow rate of molten iron at the corresponding inlet zone of the closed tuyere was set to zero.

Fig. 15(a) shows a comparison of the temperature at each temperature monitoring point during normal production and after closing some of the tuyeres. Closing the tuyeres had little effect on the temperature in the bottom area of the hearth. In the depression erosion area, the temperature decreased

significantly after closing the tuyere, and the temperatures at T3, T4, and T5 decreased by 17.3 K, 20.3 K, and 23.4 K, respectively. After the tuyere is closed, no more molten iron flows into the inlet of the corresponding position, which reduces the heat in the erosion area and promotes the formation of a solidified iron layer, which plays a local protective role.

Fig. 15(b) shows a comparison of the stresses at various monitoring points during normal production and after closing the tuyere. Closing the tuyere has little effect on the stress in the bottom area of the furnace, and the largest stress change is in the recessed erosion zone. The stresses at monitoring points S3 and S4 were reduced by 1.59 MPa and 1.34 MPa, respectively. The mitigation effect of closing the tuyere on local depression erosion is equivalent to a 10% reduction in production. Closing the tuyere effectively slows the further development of the depression erosion and ensures the production safety of the BF hearth.

IV. CONCLUSION

Based on the theory of heat transfer, computational fluid dynamics, and thermoelasticity, taking a No. 10 BF as the research object, a thermofluid-solid coupling simulation model of a BF hearth with mushroom-type depression erosion was established in this study. The common furnace protection measures were analyzed with this model, and the analysis results were consistent with furnace protection during actual production. The conclusions are as follows:

(1) The temperature and stress distributions of the hearth during normal production are high inside and low outside. The ceramic cups play an important role in protecting carbon bricks. The thermal stress of the carbon brick in the depression erosion area is relatively small and gradually decreases in a diffused state.

(2) Reducing the tapping productivity and closing the tuyere only had a large effect on the temperature and stress distribution at the depression erosion. Under the premise of meeting the production demand, the productivity can be appropriately reduced to prolong the operation life of the BF.

(3) The change in tapping temperature caused a large thermal stress change in the hearth. Therefore, when adjusting the tapping temperature, the influence of the tapping temperature on the working stability of the hearth should be fully considered.

(4) Increasing the cooling strength of the hearth can significantly reduce the thermal stress in the erosion area. It should be noted that the temperature sensitivity of the hearth gradually decreases as the cooling strength increases to a certain extent. It is necessary to match the appropriate cooling intensity for the hearth.

REFERENCES

[1] K. Shibata, Y. Kimura, M. Shimizu, and S. Inaba, "Dynamics of dead-man coke and hot metal flow in a blast furnace hearth," *ISIJ Int.*, vol. 30, no. 3, pp. 216–225, Mar. 1990.

[2] C.-E. Huang, S.-W. Du, and W.-T. Cheng, "Numerical investigation on hot metal flow in blast furnace hearth through CFD," *ISIJ Int.*, vol. 48, no. 9, pp. 1182–1187, 2008.

[3] Z.-J. Liu, J.-L. Zhang, H.-B. Zuo, and T.-J. Yang, "Recent progress on long service life design of Chinese blast furnace hearth," *ISIJ Int.*, vol. 52, no. 10, pp. 1713–1723, 2012.

[4] L. Shao and H. Saxén, "Model of blast furnace hearth drainage," *Steel Res. Int.*, vol. 83, no. 2, pp. 197–204, Feb. 2012.

[5] L. Zhang, J. Zhang, K. Jiao, X. Zhang, S. Duan, X. Wu, and J. Wang, "Hot metal flow characteristics and its contribution to hearth erosion in the early stage of blast furnace campaign," *Metall. Res. Technol.*, vol. 118, no. 4, p. 410, Jul. 2021.

[6] Z. Guo, J. Zhang, K. Jiao, Y. Zong, and Z. Wang, "Occurrence state and behavior of carbon brick brittle in a large dissected blast furnace hearth," *Steel Res. Int.*, vol. 92, no. 11, Nov. 2021, Art. no. 2100273.

[7] J. Brulin, A. Gasser, A. Rekik, E. Blond, and F. Roulet, "Thermomechanical modelling of a blast furnace hearth," *Construct. Building Mater.*, vol. 326, no. 4, Apr. 2022, Art. no. 126833.

[8] G. Wang, Z. H. Liao, Z. W. Hu, D. D. Wang, H. Bai, Z. P. Zou, and J. Xu, "Influence of the residual iron on the erosion of carbon bricks in a 4000 m^3 blast furnace hearth: From the measured properties to the proposed mechanisms," *Metall. Mater. Trans. B, Metall. Mater. Sci.*, vol. 53, no. 2, pp. 931–937, Apr. 2022.

[9] K. Takatani, T. Inada, and K. Takata, "Mathematical model for transient erosion process of blast furnace hearth," *ISIJ Int.*, vol. 41, no. 10, pp. 1139–1145, Oct. 2001.

[10] Y.-L. Li, S.-S. Cheng, P. Zhang, and S.-H. Zhou, "Sensitive influence of floating state of blast furnace deadman on molten iron flow and hearth erosion," *ISIJ Int.*, vol. 55, no. 11, pp. 2332–2341, Nov. 2015.

[11] P. C. Lai, S. W. Du, S. H. Liu, and W. T. Cheng, "Numerical investigation on effects of cooling water temperature and deadman status on thermal flow in the hearth of blast furnace during tapping shutdown," *Thermal Sci. Eng. Prog.*, vol. 23, no. 1, Jun. 2021, Art. no. 100908.

[12] M. Helle, H. Saxén, B. de Graaff, and C. van der Bent, "Wear-model-based analysis of the state of blast furnace hearth," *Metall. Mater. Trans. B, Metall. Mater. Sci.*, vol. 53, no. 1, pp. 594–603, Feb. 2022.

[13] D. W. Zhang, "Introduction and prevention of burning-through accident happened in ansteel BF hearth," (in Chinese), M.S. thesis, School Mater. Metall., Sci. Technol. Liaoning Univ., Anshan, China, 2016.

[14] T. Inada, A. Kasai, K. Nakano, S. Komatsu, and A. Ogawa, "Dissection investigation of blast furnace hearth–Kokura no. 2 blast furnace (2nd campaign)," *ISIJ Int.*, vol. 49, no. 4, pp. 470–478, Apr. 2009.

[15] Y. Deng, J.-L. Zhang, and K.-X. Jiao, "Economical and efficient protection for blast furnace hearth," *ISIJ Int.*, vol. 58, no. 7, pp. 1198–1203, Jul. 2018.

[16] Y. Zhao, D. Fu, L. W. Lherbier, Y. Chen, C. Q. Zhou, and J. G. Grindey, "Investigation of skull formation in a blast furnace hearth," *Steel Res. Int.*, vol. 85, no. 5, pp. 891–901, Dec. 2013.

[17] K. M. Komiyama, B.-Y. Guo, H. Zughbi, P. Zulli, and A.-B. Yu, "Improved CFD model to predict flow and temperature distributions in a blast furnace hearth," *Metall. Mater. Trans. B, Metall. Mater. Sci.*, vol. 45, no. 5, pp. 1895–1914, Oct. 2014.

[18] L. Y. Chen, Y. Li, and J. H. Gui, "Thermal stress of blast furnace hearth linings under erosion state," in *e-Engineering and Digital Enterprise Technology VII*. Shenyang, China: Applied Mechanics and Materials, Dec. 2013, pp. 1101–1105, doi: 10.4028/www.scientific.net/AMM.16-19.1101.

[19] J. Choi, K.-W. Han, and B.-R. Cho, "Long term high performance operation at kwangyang blast furnaces," *Revue de Métallurgie*, vol. 101, no. 3, pp. 211–218, Mar. 2004.

[20] K. Andreev, G. Louwerse, T. Peeters, and J. van der Stel, "Blast furnace campaign extension by fundamental understanding of hearth processes," *Ironmaking Steelmaking*, vol. 44, no. 2, pp. 81–91, Mar. 2016.

[21] S. V. Filatov, I. F. Kurunov, Y. M. Gordon, D. N. Tikhonov, and S. N. Grachev, "Extending the campaign life of an intensively operating blast furnace," *Metallurgist*, vol. 60, nos. 9–10, pp. 905–911, Jan. 2017.

[22] L. Wang, L. Chen, Y. Li, and J. Ma, "Numerical simulation model for evaluating protection measures of blast furnace hearth," *Processes*, vol. 10, no. 3, p. 481, Feb. 2022.

[23] W.-C. Chen and W.-T. Cheng, "Numerical simulation on forced convective heat transfer of titanium dioxide/water nanofluid in the cooling stave of blast furnace," *Int. Commun. Heat Mass Transf.*, vol. 71, pp. 208–215, Feb. 2016.

[24] L. Shao, P. Taskinen, A. Jokilaakso, H. Saxen, Y. Qu, and Z. Zou, "An experimental technique for investigating the skulling behavior in the blast furnace hearth," *Steel Res. Int.*, vol. 90, no. 2, Feb. 2019, Art. no. 1800297.

[25] K.-X. Jiao, J.-L. Zhang, Z.-J. Liu, Y. Deng, and C.-L. Chen, "Cooling phenomena in blast furnace hearth," *J. Iron Steel Res. Int.*, vol. 25, no. 10, pp. 1010–1016, Oct. 2018.
[26] X. F. Dong, P. Zulli, and M. Biasutti, "Prediction of blast furnace hearth condition: Part II—A transient state simulation of hearth condition during blast furnace shutdown," *Ironmaking Steelmaking*, vol. 47, no. 5, pp. 561–566, May 2020.
[27] Y. Deng, J. Zhang, and K. Jiao, "Residual thickness of carbon brick calculation model and systematic analysis of heat transfer," *Metall. Res. Technol.*, vol. 114, no. 2, p. 210, Apr. 2017.
[28] A. Shinotake, H. Ootsuka, N. Sasaki, and M. Ichida, "Blast furnace campaign life relating to the productivity," *Metall. Res. Technol.*, vol. 101, no. 3, pp. 203–209, Mar. 2004.
[29] K. Raipala, "Deadman and hearth phenomena in the blast furnace," *Scandin. J. Metall.*, vol. 29, no. 1, pp. 39–46, Feb. 2000.
[30] L. Shao, C. Zhang, Y. Qu, H. Saxén, and Z. Zou, "Numerical simulation of hot metal carbonization by dead-man coke in the blast furnace hearth," *Steel Res. Int.*, vol. 91, no. 2, Feb. 2020, Art. no. 1900460.
[31] Y. Zhang, R. Deshpande, D. Huang, P. Chaubal, and C. Q. Zhou, "Numerical analysis of blast furnace hearth inner profile by using CFD and heat transfer model for different time periods," *Int. J. Heat Mass Transf.*, vol. 51, nos. 1–2, pp. 186–197, Jan. 2008.
[32] B.-Y. Guo, D. Maldonado, P. Zulli, and A.-B. Yu, "CFD modelling of liquid metal flow and heat transfer in blast furnace hearth," *ISIJ Int.*, vol. 48, no. 12, pp. 1676–1685, Dec. 2008.
[33] J. Brännbacka and H. Saxén, "Model analysis of the operation of the blast furnace hearth with a sitting and floating dead man," *ISIJ Int.*, vol. 43, no. 10, pp. 1519–1527, Oct. 2003.
[34] Q. Niu, S. Cheng, W. Xu, W. Niu, and Y. Mei, "Analysis of the coke particle size distribution and porosity of deadman based on blast furnace hearth dissection," *ISIJ Int.*, vol. 59, no. 11, pp. 1997–2004, Nov. 2019.
[35] A. Koponen, M. Kataja, and J. Timonen, "Permeability and effective porosity of porous media," *Phys. Rev. E, Stat. Phys. Plasmas Fluids Relat. Interdiscip. Top.*, vol. 56, no. 3, pp. 3319–3325, Sep. 1997.
[36] Y. Li, L. Chen, L. Wang, and J. Ma, "Monitoring the safety status of a blast furnace hearth using cooling stave heat flux," *AIP Adv.*, vol. 10, no. 2, Feb. 2020, Art. no. 025308.
[37] K. Chattopadhyay, M. Isac, and R. I. L. Guthrie, "Applications of computational fluid dynamics (CFD) in iron- and steelmaking: Part 1," *Ironmaking Steelmaking*, vol. 37, no. 8, pp. 554–561, Nov. 2010.
[38] V. Panjkovic, J. S. Truelove, and P. Zulli, "Numerical modelling of iron flow and heat transfer in blast furnace hearth," *Ironmaking Steelmaking*, vol. 29, no. 5, pp. 390–400, Oct. 2002.
[39] K.-X. Jiao, J.-L. Zhang, Z.-J. Liu, F. Liu, and L.-S. Liang, "Formation mechanism of the graphite-rich protective layer in blast furnace hearths," *Int. J. Minerals, Metall., Mater.*, vol. 23, no. 1, pp. 16–24, Jan. 2016.
[40] K.-X. Jiao, J.-L. Zhang, Z.-J. Liu, C.-L. Chen, and Y.-X. Liu, "Analysis of blast furnace hearth sidewall erosion and protective layer formation," *ISIJ Int.*, vol. 56, no. 11, pp. 1956–1963, Nov. 2016.
[41] M. Sheikholeslami, "Numerical simulation of magnetic nanofluid natural convection in porous media," *Phys. Lett. A*, vol. 381, no. 5, pp. 494–503, Feb. 2017.
[42] M. Sheikholeslami, "New computational approach for exergy and entropy analysis of nanofluid under the impact of Lorentz force through a porous media," *Comput. Methods Appl. Mech. Eng.*, vol. 344, pp. 319–333, Feb. 2019.
[43] Q. Liu, P. Zhang, S. Cheng, J. Niu, and D. Liu, "Heat transfer and thermo-elastic analysis of copper steel composite stave," *Int. J. Heat Mass Transf.*, vol. 103, pp. 341–348, Dec. 2016.
[44] X. Liu, L. Chen, H. Feng, and F. Sun, "Constructal design for blast furnace wall based on the entransy theory," *Appl. Thermal Eng.*, vol. 100, pp. 798–804, May 2016.
[45] J. Ma, X. Wen, and X. Zhao, "Detection of blast furnace hearth lining erosion by multi-information fusion," *IEEE Access*, vol. 9, pp. 106192–106201, 2021.
[46] Y. Li, L. Chen, and J. Ma, "Numerical study on the relationship between the localized depression erosion of a commercial blast furnace hearth lining and the heat flux of cooling staves," *IEEE Access*, vol. 7, pp. 60984–60994, 2019.
[47] K. Jiao, J. Zhang, Q. Hou, Z. Liu, and G. Wang, "Analysis of the relationship between productivity and hearth wall temperature of a commercial blast furnace and model prediction," *Steel Res. Int.*, vol. 88, no. 9, Sep. 2017, Art. no. 1600475.

LEI WANG was born in Anshan, Liaoning, China, in 1994. He received the B.Eng. degree in mechanical design manufacture and automation from Shenyang Agricultural University, China, in 2017, and the M.Eng. degree in mechanical engineering from Northeastern University, Shenyang, China, in 2019, where he is currently pursuing the Ph.D. degree in mechanical engineering. His research interests include the safety evaluation of blast furnace hearth structure and thermal stress of blast furnace hearth.

LIANGYU CHEN was born in Weifang, Shandong, China, in 1959. He received the B.E. degree in mechanical engineering from the China University of Petroleum, Dongying, China, in 1982, and the M.E. and Ph.D. degrees in mechanical engineering from the Northeastern University, Shenyang, China, in 1986 and 1994, respectively.

Since 1997, he has been a Professor with the School of Mechanical Engineering and Automation, Northeastern University. He is the author of 12 books and more than 80 articles. His research interests include structural integrity of metallurgical equipment, mechanical power transmission, and transmission technology, and engineering equipment modeling and digital technology.

LEI ZHAO received the B.S. degree in mechanical engineering from Zaozhuang University, Shandong, China, in 2017, and the M.S. degree in mechanical engineering from the University of Science and Technology Liaoning, Anshan, China, in 2020. He is currently pursuing the Ph.D. degree in energy and power with Northeastern University, China. His research interests include granular matter dynamics and application of discrete element method in engineering machinery.

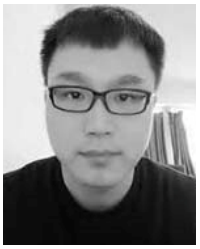

YANG LI was born in Jinzhong, Shanxi, China, in 1991. He received the B.Eng. and Ph.D. degrees in mechanical engineering from Northeastern University, Shenyang, China, in 2014 and 2020, respectively. He is currently the Chief Engineer with the State Key Laboratory of Intelligent Manufacturing of High-end Construction Machinery. His research interests include the safety evaluation of blast furnace hearth structure and abnormal erosion control of blast furnace hearth.

JIAOCHENG MA was born in Shanxi, China, in 1979. He received the B.Eng. and M.Eng. degrees in mechanical engineering and the Ph.D. degree in detection technology and automation device from Northeastern University, Shenyang, China, in 2002, 2005, and 2009, respectively. He is currently an Associate Professor with the School of Mechanical Engineering and Automation, Northeastern University. He has authored more than 20 articles. His research interests include embedded design, virtual instrument development, complex process parameter detection, modeling, and optimization control.